

The Influence of Temperature on Ozone Production under varying NO_x Conditions – a modelling study

J. Coates¹ and T. Butler¹

¹Institute for Advanced Sustainability Studies, Potsdam, Germany

January 7, 2016

Include Katie and Noelia as co-authors for providing ERA and WRF-Chem data or does an acknowledgement suffice?

Abstract

Ground-level ozone is a secondary air pollutant produced during the degradation of emitted volatile organic compounds (VOCs) and nitrogen oxides (NO_x) in the presence of sunlight. As ozone production is dependent on photochemical processes, meteorological factors such as temperature influence ozone production. Temperature directly influences ozone production through speeding up the rates of the chemical processes producing ozone and increasing the emissions of VOCs, such as isoprene, from vegetation. In this study, we used a box model to reproduce the non-linear relationship of ozone on NO_x and temperature from previous observational studies. Faster chemistry was responsible for an increase in ozone of up to 20 ppbv while increased isoprene emissions added a further 11 ppbv of ozone under high-NO_x conditions. The shorter lifetime of peroxy nitrates with increased temperature was the main contributor to the increased production of ozone with temperature. At 40 °C, the thermal decomposition of peroxy nitrates was responsible for up to 45 % of the normalised O_x production. The rate of increase in ozone with temperature from our box model simulations was about half rate of the increase in ozone with temperature over central Europe compared to both observed and WRF-Chem simulations. The missing sensitivity in our simulations compared to observations and 3D model output is related to the indirect influence of temperature on ozone production not included in our experiment.

1 Introduction

Surface-level ozone (O_3) is a secondary air pollutant formed during the photochemical degradation of volatile organic compounds (VOCs) in the presence of nitrogen oxides ($NO_x \equiv NO + NO_2$). Due to the photochemical nature of ozone production, meteorological variables such as temperature strongly influence ozone production (Jacob and Winner, 2009). Otero et al. (2015) showed that temperature was a major meteorological driver for summertime ozone in many areas of central Europe.

Temperature primarily influences ozone production in two ways: speeding up the reaction rates of many chemical reactions leading to ozone production and increasing emissions of VOCs from biogenic sources (BVOCs). In general, emissions of anthropogenic VOCs (AVOCs) are not typically dependent on temperature, however evaporative emissions of AVOCs increase with temperature (Rubin et al., 2006). The review of Pusede et al. (2015) provides further details of the temperature-dependent processes impacting ozone production.

Studies over the US (Sillman and Samson, 1995; Dawson et al., 2007; Pusede et al., 2014) noted that increased temperatures tend to lead to higher ozone levels, often exceeding local air quality guidelines. Some studies (Sillman and Samson, 1995; Dawson et al., 2007) included regional modelling to simulate the observed increases in ozone with temperature. In these studies, the increase of ozone with temperature was attributed to the shorter lifetime of PAN (peroxy acetyl nitrate) at higher temperatures and increased emissions of BVOCs, in particular isoprene, from vegetation.

Pusede et al. (2014) used an analytical model constrained by observations over San Joaquin Valley, California to infer a non-linear relationship of ozone production with temperature and NO_x , similar to the well-known non-linear relationship of ozone production on NO_x and VOC levels (Sillman, 1999). Moreover, Pusede et al. (2014) showed that temperature can be used as a surrogate for VOC levels when considering the relationship of ozone across NO_x gradients.

Environmental chamber studies have also been used to analyse the relationship of ozone with temperature. The chamber experiments of Carter et al. (1979) and Hatakeyama et al. (1991) showed increases in ozone from a VOC mix with temperature linked to increased PAN decomposition at temperatures greater than 303 K.

Despite many studies considering the effects of temperature on ozone production from an observational and chamber study perspective, there are no modelling studies (to our knowledge)

focusing on the detailed chemical processes of the influence of temperature on ozone production across NO_x gradients. Regional modelling studies have concentrated on reproducing ozone levels over regions with known meteorology and NO_x conditions then only varying the temperature. These modelling studies did not consider the relationship of ozone with NO_x with temperature. The review of Pusede et al. (2015) also highlights a lack of modelling studies looking at the non-linear relationship of ozone on temperature across NO_x gradients.

In this study, we use an idealised box model to determine how ozone levels vary with temperature across NO_x gradients. We determine whether faster chemistry or increased BVOC emissions have a greater influence on instantaneous ozone production with higher temperature at different NO_x conditions. Rasmussen et al. (2013) indicated that changing the chemical mechanism used by a model may also change the simulated ozone-temperature relationship to investigate this, we repeated all simulations using various chemical mechanisms.

2 Methodology

2.1 Model Setup

We used the MECCA box model to determine the important chemical processes for ozone production under different temperatures and NO_x conditions. The MECCA box model was set up as described in Coates and Butler (2015) and updated to include vertical mixing with the free troposphere and a diurnal cycle for the PBL height. The supplementary material includes further details of these updates.

Simulations were performed to broadly simulate urban conditions of central Europe with equinoctical conditions. The simulations started at 06:00 with a total run time of two days. Methane was fixed at 1.7 ppmv throughout the model run, carbon monoxide (CO) and ozone were initialised at 200 ppbv and 40 ppbv and then allowed to evolve freely throughout the simulation. All VOC emissions were held constant until noon of first day simulating a plume of freshly-emitted VOC.

Model runs were repeated using a temperature-dependent and temperature-independent source of BVOC emissions to determine whether increased emissions of BVOC or faster chemistry is more important for the increase of ozone with temperature. MEGAN2.1 (Guenther et al., 2012) specified the temperature-dependent BVOC emissions of isoprene and Sect. 2.3 provides further details. We considered only isoprene emissions from vegetation as isoprene emissions are the most important

on the global scale (Guenther et al., 2006). Only temperature-dependent emissions of isoprene were considered, all other emissions were constant in all simulations. In reality, many other BVOC are emitted from varying vegetation types (Guenther et al., 2006) and increased temperature can also increase AVOC emissions through increased evaporation (Rubin et al., 2006).

All simulations were repeated using different chemical mechanisms to investigate how well the relationship of ozone with temperature across NO_x gradients is represented by different representations of ozone production chemistry. The reference chemical mechanism was the near-explicit Master Chemical Mechanism, MCMv3.2, (Jenkin et al., 1997, 2003; Saunders et al., 2003; Rickard et al., 2015). The reduced chemical mechanisms in our study were Common Representative Intermediates, CRIV2 (Jenkin et al., 2008), Model for ozone and related chemical tracers, MOZART-4 (Emmons et al., 2010), Regional Acid Deposition Model, RADM2 (Stockwell et al., 1990) and the Carbon Bond Mechanism, CB05 (Yarwood et al., 2005). Coates and Butler (2015) described these chemical mechanisms and the implementation of these chemical mechanisms in MECCA. These reduced chemical mechanisms were chosen as they are commonly used by modelling groups in 3D regional and global models (Baklanov et al., 2014).

Box model simulations were performed by systematically varying the temperature between 288 and 313 K (15 – 40 °C). The only source of NO_x emissions in the box model was a constant source of NO emissions. Box model runs were performed with the NO emissions systematically varied from 5.0×10^9 to 1.5×10^{12} molecules (NO) $\text{cm}^{-2} \text{s}^{-1}$ at each temperature used in this study. At 20 °C, these NO emissions corresponded to peak NO_x mixing ratios of 0.02 ppbv and 10 ppbv respectively.

2.2 VOC Emissions

Emissions of urban AVOC over central Europe were taken from TNO-MACC_III emission inventory for the Benelux (Belgium, Netherlands and Luxembourg) region for the year 2011. TNO-MACC_III is the updated version of the TNO-MACC_II emission inventory created using the same methodology as Kuenen et al. (2014) and based upon improvements to the existing emission inventory during AQMEII-2 (Pouliot et al., 2015).

Temperature-independent emissions of isoprene and monoterpenes from biogenic sources were calculated as a fraction of the total AVOC emissions from each country in the Benelux region. This data was obtained from the supplementary data available from the EMEP (European Monitoring and Evaluation Programme) model (Simpson et al., 2012). Temperature-dependent

Table 1: Total AVOC emissions in 2011 in tonnes from each SNAP category assigned from TNO-MACC_III emission inventory and temperature-independent BVOC emissions in tonnes from Benelux region assigned from EMEP. The allocation of these emissions to MCMv3.2, CRIV2, CB05, MOZART-4 and RADM2 species is found in the supplementary material.

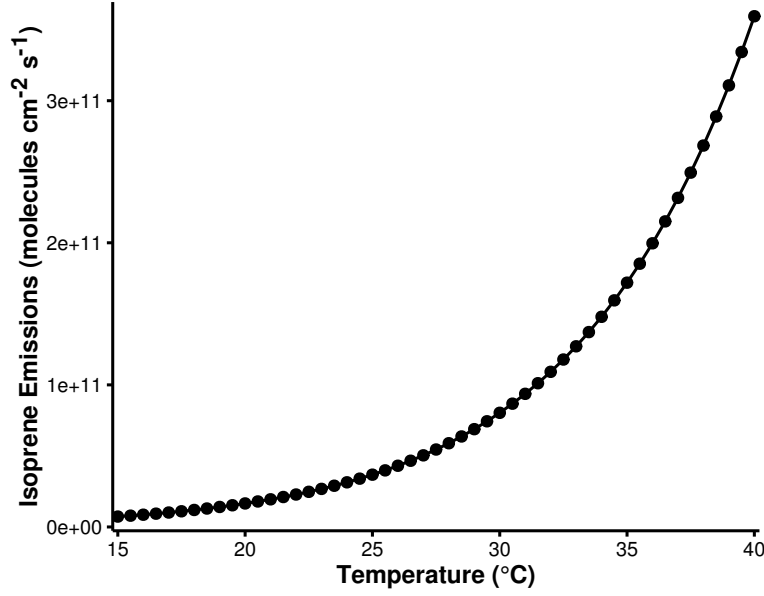
	SNAP1	SNAP2	SNAP34	SNAP5	SNAP6	SNAP71
Belgium	4494	9034	22152	5448	42809	6592
Netherlands	9140	12173	29177	8723	53535	16589
Luxembourg	121	44	208	1371	4482	1740
Total	13755	21251	62648	15542	100826	24921
	SNAP72	SNAP73	SNAP74	SNAP8	SNAP9	BVOC
Belgium	2446	144	210	6448	821	7042
Netherlands	3230	1283	1793	10067	521	1462
Luxembourg	1051	6	324	643	0	2198
Total	6727	1433	2327	17158	1342	10702

emissions of isoprene are detailed in Sect. 2.3.

AVOC emissions were allocated to SNAP (Selected Nomenclature for Air Pollution) source categories. Table 1 shows the tonnes of VOC emissions from each SNAP category and the temperature-independent BVOC emissions. These categorised AVOC emissions were assigned to chemical species and groups based on the country specific profiles for Belgium, the Netherlands and Luxembourg provided by TNO. Most individual chemical species are represented by the MCMv3.2, otherwise the individual contributions of a group of VOC were further split into individual components using the detailed speciation of Passant (2002). For example, ‘xylenes’ are one of the component chemical groups in many SNAP categories but the MCMv3.2 treats xylenes as the individual isomers (m-, o-, p-xylene) and the contributions of the individual isomers to a SNAP category was provided by Passant (2002). This approach was also used in von Schneidemesser et al. (2015) to allocate AVOC emissions from different solvent sector speciations to MCMv3.2 species.

The VOC emissions represented by the MCMv3.2 were mapped to the mechanism species representing VOC emissions in each reduced chemical mechanism based on the recommendations of the source literature. The VOC emissions in the reduced chemical mechanisms were weighted by the carbon numbers of the MCMv3.2 species and the emitted mechanism species. The supplementary data outlines the primary VOC and calculated emissions with each chemical mechanism.

Figure 1: The estimated isoprene emissions (molecules isoprene $\text{cm}^{-2} \text{s}^{-1}$) using MEGAN2.1 at each temperature used in the study.



2.3 Temperature Dependent Isoprene Emissions

Temperature-dependent emissions of isoprene were estimated using the MEGAN2.1 algorithm for calculating the emissions of VOC from vegetation (Guenther et al., 2012). Emissions from plants are dependent on variables including temperature, radiation and age but for the purpose of our study all variables except temperature were held constant.

The MEGAN2.1 parameters were chosen to give similar isoprene mixing ratios at 20 °C to the temperature-independent emissions of isoprene in order to compare the effects of increased isoprene emissions with temperature. The estimated emissions of isoprene with MEGAN2.1 using these assumptions, are illustrated in Fig. 1 and show the expected exponential increase in isoprene emissions with temperature (Guenther et al., 2006).

The estimated emissions of isoprene at 20 °C lead to 0.07 ppbv of isoprene in our simulations while at 30 °C, the increased emissions of isoprene using MEGAN2.1 estimations lead to 0.35 ppbv of isoprene in the model. A measurement campaign over Essen, Germany (Wagner and Kuttler, 2014) measured 0.1 ppbv of isoprene at temperature 20 °C and 0.3 ppbv of isoprene were measured at 30 °C. The similarity of the simulated and observed isoprene mixing ratios indicates that the MEGAN2.1 variables chosen for calculating the temperature-dependent emissions of isoprene were suitable for simulating urban conditions over central Europe.

Table 2: Increase in ozone mixing ratio (ppbv) due to chemistry and emissions at 40 °C from reference temperature (20 °C) in the NO_x-regimes of Fig. 3.

Chemical Mechanism	Source of Difference	Increase in Ozone at 40 °C from 20 °C (ppbv)		
		Low-NO _x	Maximal-O ₃	High-NO _x
MCMv3.2	Chemistry	6.8	12.5	15.2
	Emissions	4.6	7.7	10.6
CRIV2	Chemistry	6.0	11.1	13.7
	Emissions	4.8	7.9	10.8
MOZART-4	Chemistry	6.0	10.2	12.3
	Emissions	4.1	6.7	10.0
CB05	Chemistry	9.3	16.0	19.9
	Emissions	4.6	7.4	9.8
RADM2	Chemistry	8.6	14.1	17.3
	Emissions	3.8	5.7	7.8

3 Results and Discussion

3.1 Ozone as a Function of NO_x and Temperature

Figure 2 depicts the maximum mixing ratio of ozone as a function of the total NO_x emissions on the first day of simulations and temperature when using a temperature-independent and temperature-dependent source of isoprene emissions for each chemical mechanism. A non-linear relationship of ozone mixing ratios with NO_x and temperature is reproduced by each chemical mechanism. This non-linear relationship is similar to that determined by Pusede et al. (2014) using an analytical model constrained to observational measurements over the San Joaquin Valley in California.

Higher ozone mixing ratios are produced when using a temperature-dependent source of isoprene emissions in Fig. 2. The highest mixing ratios of ozone are produced at high temperatures and high emissions of NO_x regardless of the source of isoprene emissions. Conversely, the least amount of ozone is produced with low emissions of NO_x over the whole temperature range (15 – 40 °C) when using both a temperature-independent and temperature-dependent source of isoprene emissions.

The contours of ozone mixing ratios as a function of NO_x and temperature can be split into three NO_x regimes (Low-NO_x, Maximal-O₃ and High-NO_x), similar to the NO_x regimes defined for the non-linear relationship of ozone with VOC and NO_x. The Low-NO_x regime corresponds to regions with little increase in ozone with temperature, also called NO_x-sensitive regime. The High-NO_x (or NO_x-saturated) regime is when ozone levels increase rapidly with temperature and the contour ridges correspond to regions of maximal ozone production and we call this the

Figure 2: Contours of maximum ozone mixing ratios as a function of the total NO_x emissions on the first day and temperature for each chemical mechanism using a temperature-dependent and temperature-independent source of isoprene emissions.

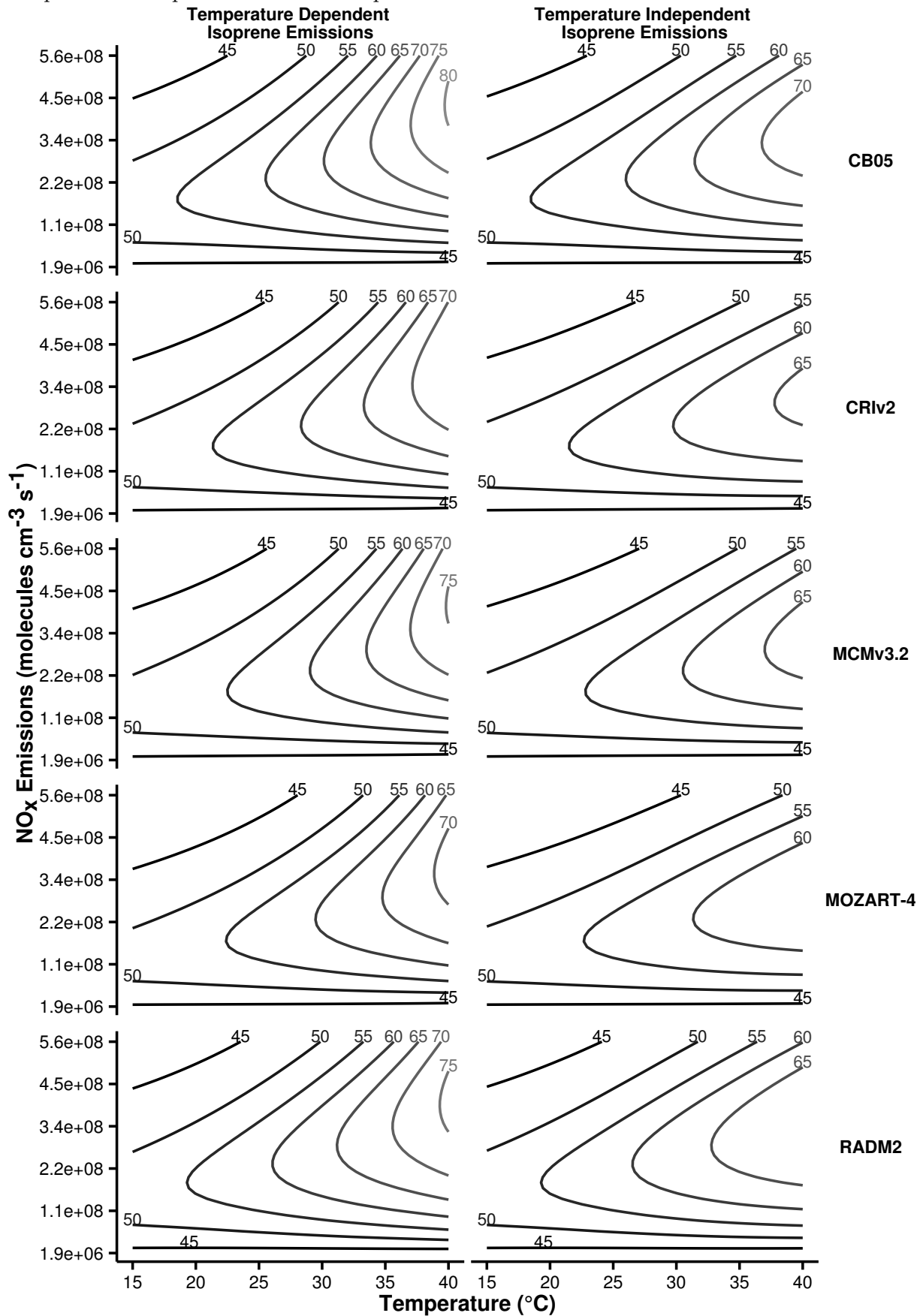
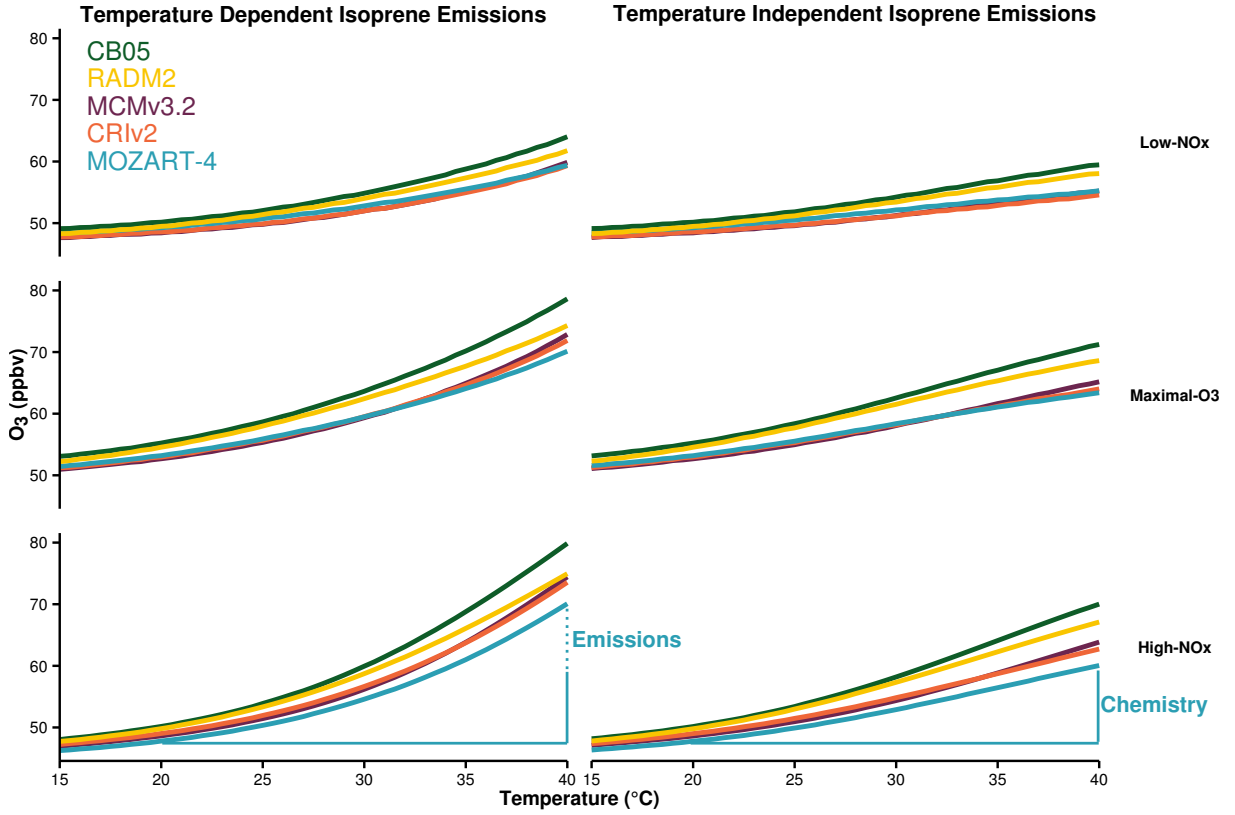


Figure 3: Ozone mixing ratios at each temperature are allocated to different NO_x -regimes of Fig. 2. The differences in ozone mixing ratios due to chemistry (solid line) and emissions (dotted line) are represented graphically for MOZART-4 with High- NO_x conditions and summarised in Table 2, the approach was used to calculate the differences with each chemical mechanism.



Maximal- O_3 regime. Pusede et al. (2014) showed that temperature can be used as a proxy for VOC, thus we assigned the ozone mixing ratios from each box model simulation to a NO_x regimes based on the ratio of HNO_3 to H_2O_2 used by Sillman (1995) to designate ozone to NO_x regimes based on NO_x and VOC levels.

Fig. 3 illustrates the mean ozone mixing ratio at each temperature in the NO_x regimes for each chemical mechanism and each source of isoprene emissions. The absolute increase in ozone at 40 °C from 20 °C due to faster chemistry is the difference between ozone mixing ratios at 40 °C and 20 °C when using a temperature-independent source of isoprene emissions. When using a temperature-dependent source of isoprene emissions, the difference in ozone mixing ratios at 40 °C from 20 °C minus the increase due to faster chemistry, gives the absolute increase in ozone due to increased isoprene emissions. These differences are represented graphically in Fig. 3 and summarised in Table 2.

Table 2 shows that the absolute increase in ozone with temperature due to faster chemistry is larger than the absolute increase in ozone due to increased isoprene emissions for each chemical mechanism and each NO_x regime. The absolute increase in ozone is largest with High- NO_x

conditions and lowest with Low-NO_x conditions (Fig. 3 and Table 2). The increase in ozone mixing ratio at 40 °C from 20 °C due to faster chemistry with High-NO_x conditions is almost double that with Low-NO_x conditions. We determine the chemical processes responsible for the increases in ozone mixing ratios with temperature by analysing O_x production budgets in Sect. 3.2.

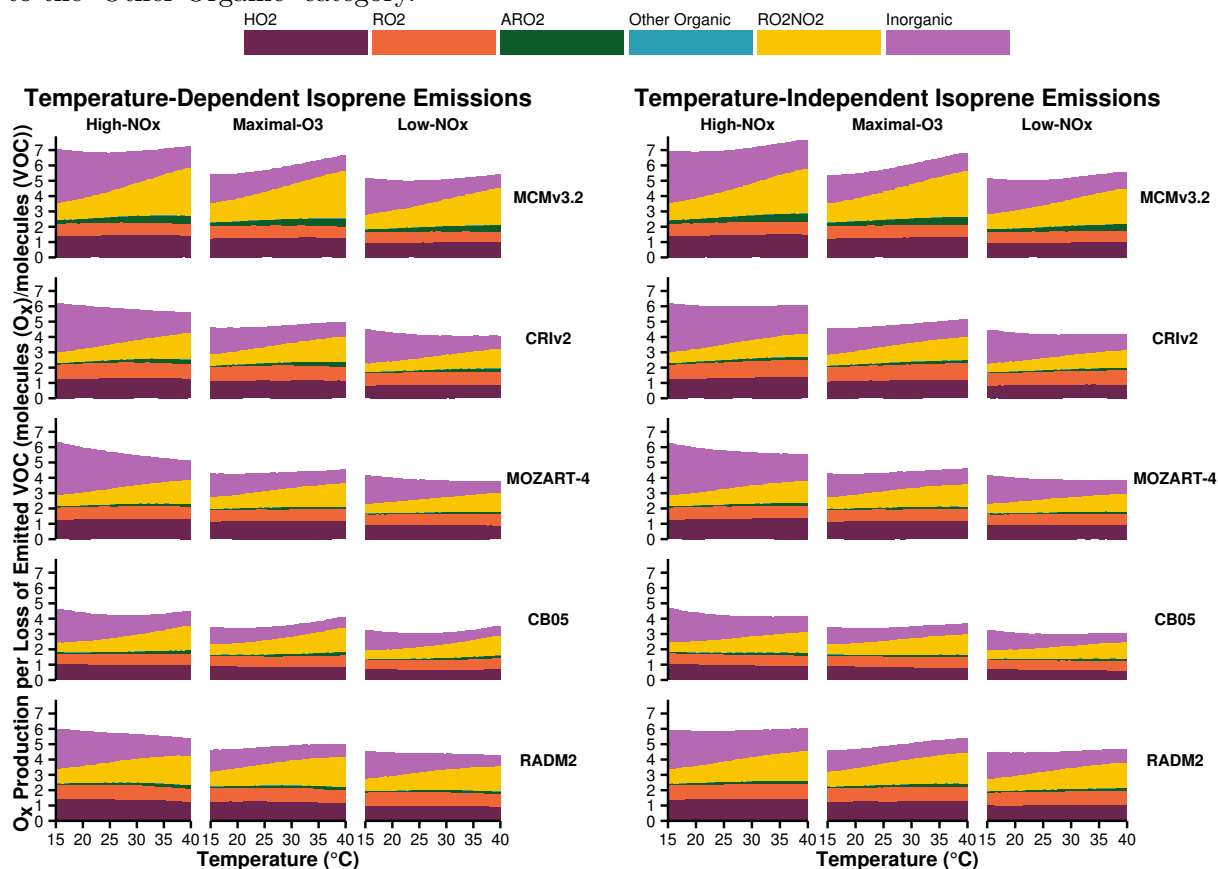
The largest differences in ozone mixing ratios using the reduced chemical mechanisms (CRIV2, MOZART-4, CB05 and RADM2) from the MCMv3.2 occur in the Maximal-O₃ and High-NO_x regimes. Table 2 also indicates that all reduced chemical mechanisms except RADM2 have similar increases in ozone due to increased isoprene emissions to MCMv3.2. RADM2 produces 3 ppbv less ozone than the MCMv3.2 due to increased isoprene emissions in each NO_x regime, indicating that this difference is due to how isoprene degradation chemistry is treated in RADM2.

The Tagged Ozone Production Potential (TOPP) defined in Butler et al. (2011) is a measure of the number of molecules of ozone produced per molecule of VOC emitted. Coates and Butler (2015) compared ozone production in different chemical mechanisms to the MCMv3.2 using TOPPs and showed that less ozone is produced per molecule of isoprene emitted using RADM2 than with MCMv3.2. The degradation of isoprene has been extensively studied and it is well-known that methyl vinyl ketone (MVK) and methacrolein are signatures of isoprene degradation. All chemical mechanisms in our study except RADM2 explicitly represent MVK and methacrolein (or in the case of CB05, a lumped species representing both these secondary degradation products). RADM2 does not represent methacrolein and the mechanism species representing ketones (KET) represents a mixture of acetone and methyl ethyl ketone (MEK). Thus the secondary degradation of isoprene in RADM2 is unable to represent the ozone production from the further degradation of the signature secondary degradation products of isoprene, MVK and methacrolein. Updated versions of RADM2, RACM (Stockwell et al., 1997) and RACM2 (Goliff et al., 2013), sequentially included methacrolein and MVK and with these updates the TOPP value of isoprene approached that of the MCMv3.2 (Coates and Butler, 2015).

3.2 Ozone Production Budgets

The total day-time production budgets of O_x (\equiv O₃ + NO₂ + O) normalised by the total rate of oxidation of the emitted VOC are displayed in Fig. 4. The O_x production budgets are assigned to each NO_x regime for each chemical mechanism and source of isoprene emissions. The budgets are allocated to the major sources, where ‘HO2’, ‘RO2’, ‘ARO2’ represent the reactions of NO

Figure 4: Day-time O_x production budgets normalised by the total oxidation rate of emitted VOC in the NO_x -regimes of Fig. 3. The budgets are allocated to categories of inorganic reactions, peroxy nitrate (RO_2NO_2) decomposition, reactions of NO with HO_2 , alkyl peroxy radicals (RO_2) and acyl peroxy radicals (ARO_2). All other reactions contributing to O_x budgets are allocated to the ‘Other Organic’ category.



with HO_2 , alkyl peroxy radicals and acyl peroxy radicals respectively. ‘ RO_2NO_2 ’ represents the thermal decomposition of peroxy nitrates, ‘Inorganic’ represents all inorganic contributions to O_x production (primarily the de-excitation of O^1D to O) and any other remaining organic reactions producing O_x are included in the ‘Other Organic’ category.

In Fig. 4, a similar number of molecules of O_x per molecule of emitted VOC oxidised are produced in High- NO_x conditions when using either temperature-dependent or temperature-independent isoprene emissions for each chemical mechanism, the same occurs for the Maximal- O_3 and Low- NO_x regimes. Thus the increases in ozone production due to increased emissions of isoprene with temperature are balanced by the faster oxidation rates at higher temperatures. The largest amount of O_x is produced in the High- NO_x regime and the lowest amount of O_x is produced in the Low- NO_x regime, mirroring the O_3 mixing ratios in the different NO_x regimes in Fig. 3. For example, MCMv3.2 produces seven molecules of O_x per molecule of emitted VOC oxidised in High- NO_x conditions decreasing to about six and five molecules of O_x

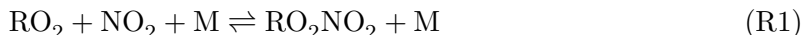
per molecule of emitted VOC oxidised in the Maximal-O₃ and Low-NO_x regimes.

Thermal decomposition of RO₂NO₂ contributes the most to the normalised O_x production at higher temperatures in Fig. 4, this contribution shows a strong dependency on temperature and is analysed further in Sect. 3.2.1. The contributions of the reaction of NO with peroxy radicals (HO₂, RO₂ and ARO₂ in Fig. 4) to the normalised production of O_x do not increase strongly with temperature indicating that the faster oxidation of emitted VOC at higher temperatures produces more peroxy radicals which when reacting NO fuels O_x production.

The reduced chemical mechanisms produce up to two molecules of O_x per molecule of emitted VOC oxidised less than the MCMv3.2 in each NO_x regime despite the reduced chemical mechanisms producing similar absolute amounts of ozone to the MCMv3.2 (Fig. 2 and Fig. 3). At high temperatures, up to 86 % of the total difference in the normalised O_x production using the reduced chemical mechanisms from the MCMv3.2 is due to differences in the contribution from peroxy nitrate (RO₂NO₂) decomposition.

3.2.1 Peroxy Nitrates

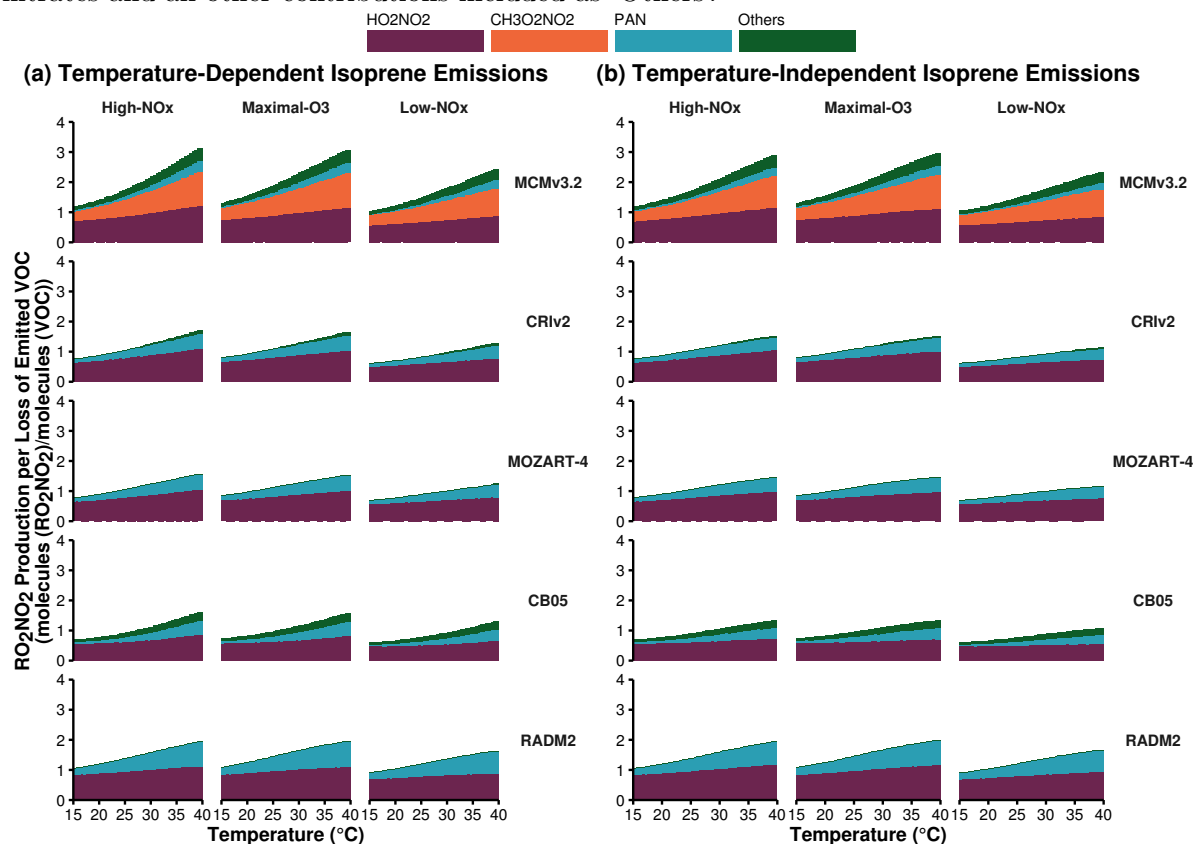
Peroxy nitrates are formed from the reactions of peroxy radicals (RO₂) with NO₂ (R1) and are an important reservoir species for both peroxy radicals and NO_x.



The chemical bond of RO₂NO₂ is relatively weak and thermal decomposition is the most important chemical process with the rate of thermal decomposition increasing strongly with temperature. At low temperatures, RO₂NO₂ can accumulate and be transported downwind of emissions of the sources of its precursors (VOC and NO_x) and after thermal decomposition the release of NO₂ and peroxy radicals can promote production of O₃ (Moxim et al., 1996).

Peroxy nitrates are formed from both alkyl and acyl peroxy radicals produced during the secondary degradation of emitted VOC. The most important alkyl peroxy nitrates are pernitric acid (HO₂NO₂) and methylperoxy nitrate (CH₃O₂NO₂), while peroxy acetyl nitrate (PAN, CH₃C(O)O₂NO₂) and peroxy propionyl nitrate (PPN, C₂H₅C(O)O₂NO₂) are important acyl peroxy nitrates. The alkyl peroxy nitrates have a weaker RO₂–NO₂ bond than acyl peroxy nitrates hence alkyl peroxy nitrates have a shorter lifetime than acyl peroxy nitrates. At 298 K, the lifetime of CH₃O₂NO₂ is 0.5 seconds while PAN has a lifetime of 51 minutes (Orlando and

Figure 5: Day-time RO_2NO_2 production budgets normalised by the total oxidation rate of emitted VOC in the NO_x -regimes of Fig. 3. The total budgets are allocated to the most important peroxy nitrates and all other contributions included as ‘Others’.



Tyndall, 2012).

Each chemical mechanism used in our study represents HO_2NO_2 and PAN, although in many reduced chemical mechanisms the PAN mechanism species represents $\text{CH}_3\text{C}(\text{O})\text{O}_2\text{NO}_2$ and other acyl peroxy nitrates. This representation of PAN in reduced chemical mechanisms can overestimate PAN levels compared to more detailed chemical mechanisms (Luecken et al., 1999). The near-explicit MCMv3.2 represents a range of peroxy nitrates including $\text{CH}_3\text{O}_2\text{NO}_2$ and about 280 acyl peroxy nitrates.

Figure 5 displays the normalised production budgets of RO_2NO_2 by the total oxidation rate of the emitted VOC for each chemical mechanism in each NO_x regime with a temperature-independent and temperature-dependent source of isoprene emissions. The contribution of $\text{CH}_3\text{O}_2\text{NO}_2$ to normalised RO_2NO_2 production in MCMv3.2 is missing from the budgets of each reduced chemical mechanism as $\text{CH}_3\text{O}_2\text{NO}_2$ is not represented in any of the reduced chemical mechanisms. In fact when removing the contribution of $\text{CH}_3\text{O}_2\text{NO}_2$ to normalised RO_2NO_2 production in MCMv3.2, the normalised RO_2NO_2 production of the reduced chemical mechanisms is similar to that in the MCMv3.2 for each NO_x regime and regardless of

Table 3: Slopes (m_{O_3-T} in ppbv per $^{\circ}C$) of the linear fit to the ozone-temperature correlations in Fig. 6

(a) Slope of linear fit of the ERA-Interim observational data and WRF-Chem model output using MOZART-4 and RADM2 chemistry over central and eastern Germany and western and central Poland.

	Germany	Poland
ERA-Interim	2.15	1.94
WRF-Chem with MOZART-4	2.05	2.00
WRF-Chem with RADM2	1.78	1.77

(b) Slope of linear fit of box model experiments for each chemical mechanism, source of isoprene emissions allocated to the three NO_x -regimes.

Mechanism	Isoprene Emissions	Low- NO_x	Maximal- O_3	High- NO_x
MCMv3.2	Temperature Dependent	0.42	0.74	0.93
	Temperature Independent	0.28	0.51	0.59
CRIv2	Temperature Dependent	0.40	0.71	0.90
	Temperature Independent	0.25	0.47	0.55
MOZART-4	Temperature Dependent	0.38	0.65	0.81
	Temperature Independent	0.25	0.44	0.49
CB05	Temperature Dependent	0.52	0.89	1.12
	Temperature Independent	0.39	0.67	0.79
RADM2	Temperature Dependent	0.48	0.79	0.97
	Temperature Independent	0.37	0.61	0.70

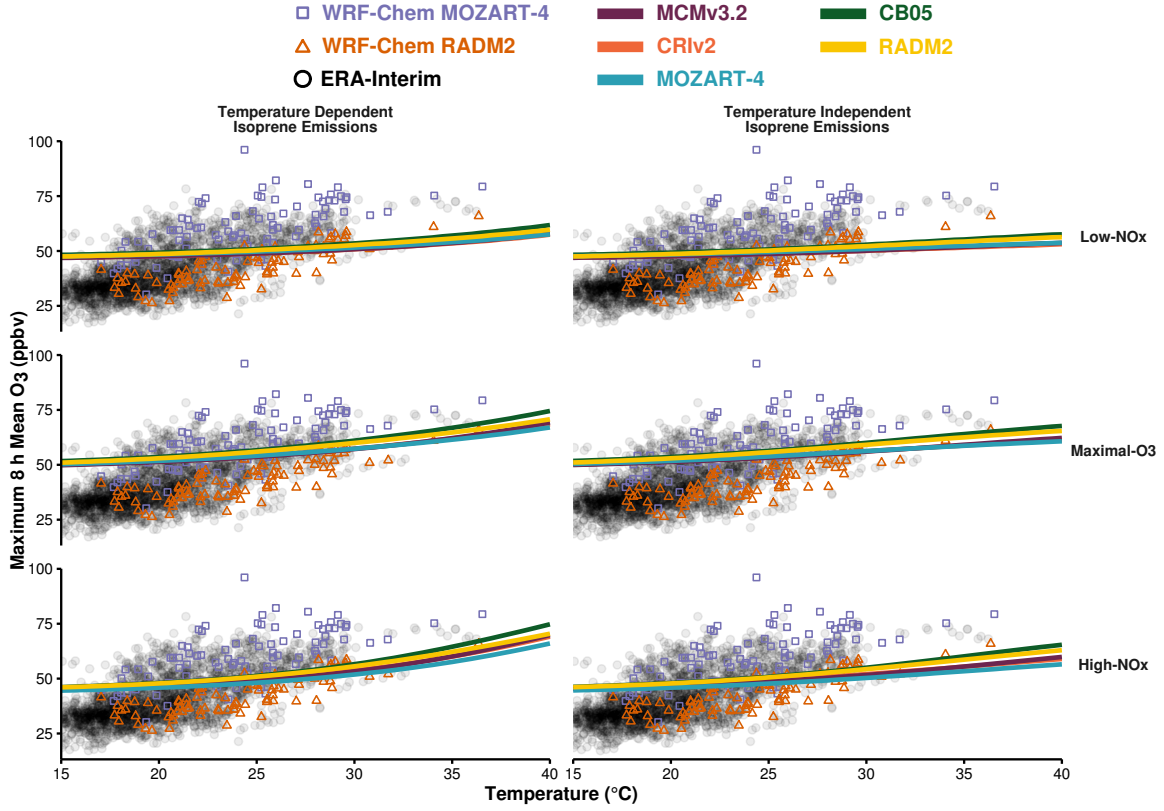
isoprene source. Including $CH_3O_2NO_2$ chemistry in reduced chemical mechanisms would improve the representation of the total RO_2NO_2 production having the added benefit of improving the representation of O_x production budgets in Fig. 4.

3.3 Comparison to Observations and 3D Model Simulations

This section compares the results from our idealised box model simulations to real-world observations and model output from a 3D model verifying the applicability of our results to more realistic atmospheric conditions. Otero et al. (2015) showed that over the summer (JJA) months, temperature is the main meteorological driver of ozone production over many regions of central Europe using the observational data set of the ERA-Interim re-analysis of Schnell et al. (2015). This data set includes the daily maximum temperature and daily maximum 8 h mean of ozone for the years 1998–2012 over Europe. Model output from the 3D WRF-Chem regional model set-up over the European domain for simulations of the year 2007 using MOZART-4 and RADM2 chemistry from Mar (2015) was used to further compare the box model simulations to a model including more meteorological processes than the box model.

Figure 6: The maximum 8 h mean ozone from the box model simulations allocated to the different NO_x regimes for each chemical mechanisms (solid lines). The box model ozone-temperature correlation is compared to the summer 2007 ERA-Interim data (black circles) and WRF-Chem output using MOZART-4 (purple boxes) and RADM2 (orange triangles).

(a) Ozone-Temperature correlation over central and eastern Germany



(b) Ozone-Temperature correlation over central and western Poland

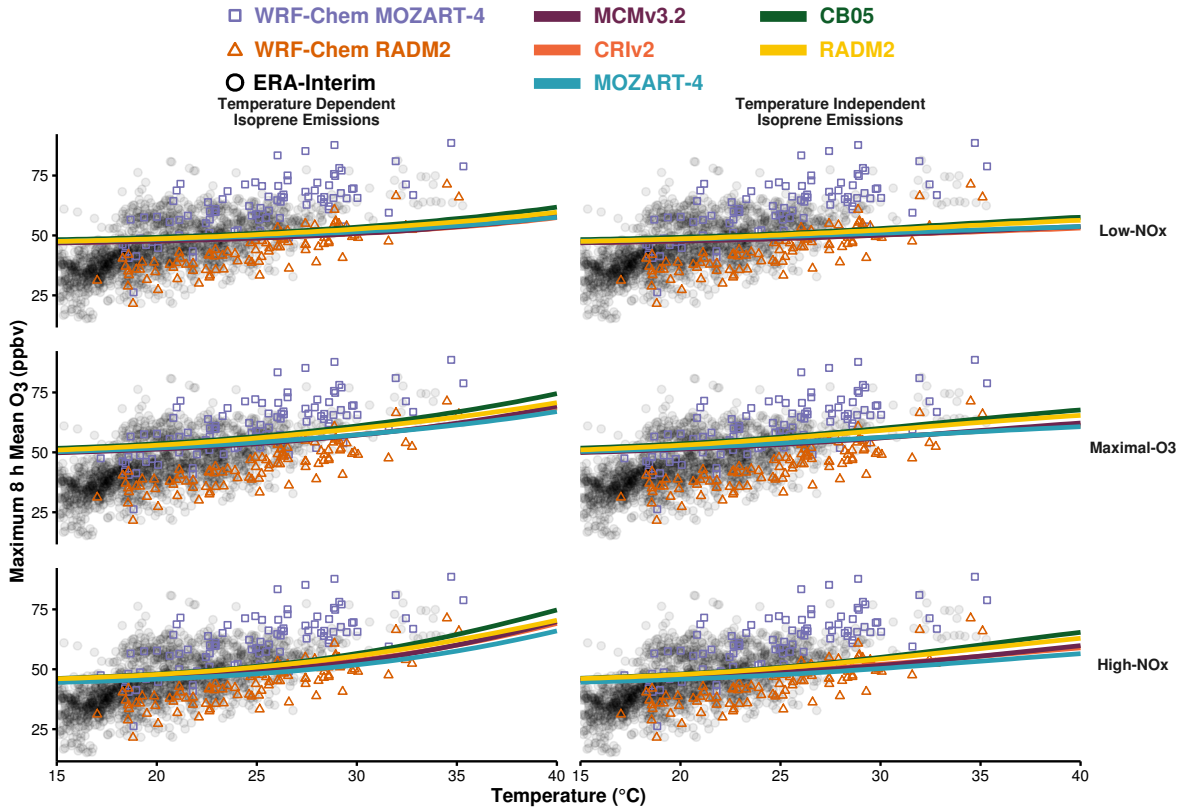


Figure 6 compares the summer data of 2007 from observations (ERA-Interim), WRF-Chem simulations and the maximum 8 h mean ozone from the box model simulations using a temperature-independent and temperature-dependent source of isoprene emissions for each chemical mechanism and allocated to the different NO_x -regimes. In Fig. 6, only days where the daily maximum temperature corresponded to the temperature range in our study (15–40 °C) were considered from the ERA-Interim observational data set. We selected two regions of the gridded domains of the observations and WRF-Chem output, central and eastern Germany (Fig. 6a) and central and western Poland (Fig. 6b), as the summertime ozone values in these regions are correlated with temperature (Otero et al., 2015). Table 3 summarises the slopes ($m_{\text{O}_3\text{-T}}$) of the linear fits of all the ozone-temperature correlations displayed in Fig. 6 in ppbv of ozone per °C determining the rate of change of ozone with temperature.

The spread of the ERA-Interim ozone-temperature values over both Germany and Poland are generally captured by the combined WRF-Chem simulations with both MOZART-4 and RADM2 chemistry. However, the ozone-temperature data from WRF-Chem using MOZART-4 chemistry reproduces the higher ozone values with temperature from ERA-Interim but not the lower values. On the other hand, WRF-Chem with RADM2 only reproduces the lower ozone values of the ERA-Interim data. The differences between the ozone produced using WRF-Chem with MOZART-4 and RADM2 shall be addressed in Mar (2015). The rate of change of ozone with temperature from the WRF-Chem simulations using MOZART-4 is closer to the ERA-Interim data than the WRF-Chem simulations using RADM2 (Table 3a).

The box model simulations using a temperature-independent source of isoprene emissions do not reproduce the range of observed ozone-temperature values, also indicated by the lower $m_{\text{O}_3\text{-T}}$ values of the box model simulations than ERA-Interim in Table 3. Also, the differences in ozone production from the different chemical mechanisms with the box model are insignificant compared to the spread of the ERA-Interim and WRF-Chem data. When using a temperature-dependent source of isoprene emissions in the box model, the rate of change of ozone with temperature in the box model approaches that of the observed data.

High- NO_x conditions with a temperature-dependent source of isoprene produce the most similar ozone-temperature slope to the observational data but this is still lower by a factor of two than the observed ozone-temperature slope. In particular, the box model simulations over-predict the ozone values at lower temperatures and under-predict the ozone values at higher temperatures compared to the ERA-Interim data, regardless of the chemical mechanism. Similarly, the rate

of change of ozone with temperature in the box model is less-sensitive than WRF-Chem using MOZART-4 or RADM2 chemistry.

The main reason for the box model simulations being less sensitive to temperature than the observations is related to the set-up of the experiments compared to observations. Observations consider the total effect of temperature on ozone, while models represent the individual effects of temperature on ozone. In other words, observational studies look at the total derivative of ozone with temperature while models look at the partial derivatives of the temperature-dependent processes influencing ozone (Rasmussen et al., 2013).

$$\frac{d[\text{O}_3]}{dT} = \frac{\partial[\text{O}_3]}{\partial[\text{BVOC}]} \frac{\partial[\text{BVOC}]}{\partial T} + \frac{\partial[\text{O}_3]}{\partial \text{Chemistry}} \frac{\partial \text{Chemistry}}{\partial T} + \frac{\partial[\text{O}_3]}{\partial \text{Stagnation}} \frac{\partial \text{Stagnation}}{\partial T} + \dots$$

In our simulations, we focused on instantaneous production of ozone from a freshly-emitted source of VOC not considering stagnant atmospheric conditions. In these atmospheric conditions, the ozone built-up from the previous day is not transported away from the region and can lead to increased ozone levels with the production of fresh ozone from new emissions. Otero et al. (2015) showed that the previous day’s ozone was also an important driver for observed ozone production over Europe. 3D models such as WRF-Chem that simulate more realistic atmospheric conditions would play a valuable role for future work that would also include stagnant conditions.

4 Conclusions

In this study, we determined the effects of temperature on ozone production using a box model over a range of temperatures and NO_x conditions using a temperature-independent and temperature-dependent source of isoprene emissions. These simulations were repeated using reduced chemical mechanism schemes (CRIV2, MOZART-4, CB05 and RADM2) typically used in 3D models and compared to the near-explicit MCMv3.2 chemical mechanism. Each chemical mechanism produced a non-linear relationship of ozone with temperature and NO_x with the most ozone produced at high temperatures and high emissions of NO_x . Conversely, lower NO_x levels led to a minimal increase of ozone with temperature. Thus air quality in a future with higher temperatures predicted with climate change would benefit from dramatically reducing NO_x emissions.

Faster chemistry at higher temperatures was responsible for a greater absolute increase in ozone than increased isoprene emissions. Faster thermal decomposition of peroxy nitrates at

higher temperatures contributed the most to ozone production with each chemical mechanism and all NO_x conditions. The contribution of peroxy nitrates using reduced chemical mechanisms was larger than in MCMv3.2 due to the inclusion of methylperoxy nitrate ($\text{CH}_3\text{O}_2\text{NO}_2$) chemistry that is not included in any other chemical mechanism used in this study. Including methylperoxy nitrate chemistry in reduced chemical mechanisms would minimise the differences in the production of ozone from reduced chemical mechanisms to the MCMv3.2 at higher temperatures.

The rate of change of ozone with temperature using observational data (ERA-Interim) over Europe was twice as high as when using the box model. This was due to the box model not representing stagnant atmospheric conditions that are inherently included in observational data and models including meteorology, such as WRF-Chem. Future work looking at the influence of temperature on ozone should include stagnant conditions to represent more realistic atmospheric conditions. Any modelling work addressing this should also consider a range of NO_x conditions as this strongly influenced the amount of ozone produced in our study.

References

- A. Baklanov, K. Schlünzen, P. Suppan, J. Baldasano, D. Brunner, S. Aksoyoglu, G. Carmichael, J. Douros, J. Flemming, R. Forkel, S. Galmarini, M. Gauss, G. Grell, M. Hirtl, S. Joffre, O. Jorba, E. Kaas, M. Kaasik, G. Kallos, X. Kong, U. Korsholm, A. Kurganskiy, J. Kushta, U. Lohmann, A. Mahura, A. Manders-Groot, A. Maurizi, N. Moussiopoulos, S. T. Rao, N. Savage, C. Seigneur, R. S. Sokhi, E. Solazzo, S. Solomos, B. Sørensen, G. Tsegas, E. Vignati, B. Vogel, and Y. Zhang. Online coupled regional meteorology chemistry models in Europe: current status and prospects. *Atmospheric Chemistry and Physics*, 14(1):317–398, 2014.
- T.M. Butler, M.G. Lawrence, D. Taraborrelli, and J. Lelieveld. Multi-day ozone production potential of volatile organic compounds calculated with a tagging approach. *Atmospheric Environment*, 45(24):4082 – 4090, 2011.
- William P. L. Carter, Arthur M. Winer, Karen R. Darnall, and James N. Pitts Jr. Smog chamber studies of temperature effects in photochemical smog. *Environmental Science & Technology*, 13(9):1094–1100, 1979.
- J. Coates and T. M. Butler. A comparison of chemical mechanisms using tagged ozone production potential (TOPP) analysis. *Atmospheric Chemistry and Physics*, 15(15):8795–8808, 2015.

373 John P. Dawson, Peter J. Adams, and Spyros N. Pandis. Sensitivity of ozone to summertime
 374 climate in the eastern USA: A modeling case study . *Atmospheric Environment*, 41(7):1494 –
 375 1511, 2007.

376 L. K. Emmons, S. Walters, P. G. Hess, J.-F. Lamarque, G. G. Pfister, D. Fillmore, C. Granier,
 377 A. Guenther, D. Kinnison, T. Laepple, J. Orlando, X. Tie, G. Tyndall, C. Wiedinmyer, S. L.
 378 Baughcum, and S. Kloster. Description and evaluation of the Model for Ozone and Related
 379 chemical Tracers, version 4 (MOZART-4). *Geoscientific Model Development*, 3(1):43–67, 2010.

380 Wendy S. Goliff, William R. Stockwell, and Charlene V. Lawson. The regional atmospheric
 381 chemistry mechanism, version 2. *Atmospheric Environment*, 68:174 – 185, 2013.

382 A. Guenther, T. Karl, P. Harley, C. Wiedinmyer, P. I. Palmer, and C. Geron. Estimates of global
 383 terrestrial isoprene emissions using MEGAN (Model of Emissions of Gases and Aerosols from
 384 Nature). *Atmospheric Chemistry and Physics*, 6(11):3181–3210, 2006.

385 A. B. Guenther, X. Jiang, C. L. Heald, T. Sakulyanontvittaya, T. Duhl, L. K. Emmons, and
 386 X. Wang. The Model of Emissions of Gases and Aerosols from Nature version 2.1 (MEGAN2.1):
 387 an extended and updated framework for modeling biogenic emissions. *Geoscientific Model*
 388 *Development*, 5(6):1471–1492, 2012.

389 Shiro Hatakeyama, Hajime Akimoto, and Nobuaki Washida. Effect of temperature on the
 390 formation of photochemical ozone in a propene-nitrogen oxide (NO_x)-air-irradiation system.
 391 *Environmental Science & Technology*, 25(11):1884–1890, 1991.

392 Daniel J. Jacob and Darrell A. Winner. Effect of climate change on air quality. *Atmospheric*
 393 *Environment*, 43(1):51 – 63, 2009. Atmospheric Environment - Fifty Years of Endeavour.

394 M. E. Jenkin, S. M. Saunders, V. Wagner, and M. J. Pilling. Protocol for the development of the
 395 Master Chemical Mechanism, MCM v3 (Part B): tropospheric degradation of aromatic volatile
 396 organic compounds. *Atmospheric Chemistry and Physics*, 3(1):181–193, 2003.

397 M.E. Jenkin, L.A. Watson, S.R. Utembe, and D.E. Shallcross. A Common Representative
 398 Intermediates (CRI) mechanism for VOC degradation. Part 1: Gas phase mechanism development.
 399 *Atmospheric Environment*, 42(31):7185 – 7195, 2008.

400 Michael E. Jenkin, Sandra M. Saunders, and Michael J. Pilling. The tropospheric degradation of

401 volatile organic compounds: a protocol for mechanism development. *Atmospheric Environment*,
402 31(1):81 – 104, 1997.

403 J. J. P. Kuenen, A. J. H. Visschedijk, M. Jozwicka, and H. A. C. Denier van der Gon.
404 TNO-MACC_II emission inventory; a multi-year (2003–2009) consistent high-resolution european
405 emission inventory for air quality modelling. *Atmospheric Chemistry and Physics*, 14(20):
406 10963–10976, 2014.

407 D.J. Luecken, G.S. Tonnesen, J.E. Sickles, and II. Differences in NO_y speciation predicted by
408 three photochemical mechanisms. *Atmospheric Environment*, 33(7):1073 – 1084, 1999.

409 Kathleen A. Mar. WRF-Chem Simulations over Europe: Model Evaluation and Chemical
410 Mechanism Comparison. *In Preparation*, 2015.

411 W. J. Moxim, H. Levy, and P. S. Kasibhatla. Simulated global tropospheric PAN: Its transport
412 and impact on NO_x. *Journal of Geophysical Research: Atmospheres*, 101(D7):12621–12638, 1996.

413 John J. Orlando and Geoffrey S. Tyndall. Laboratory studies of organic peroxy radical chemistry:
414 an overview with emphasis on recent issues of atmospheric significance. *Chem. Soc. Rev.*, 41:
415 6294–6317, 2012.

416 N. Otero, J. Sillmann, J. L. Schnell, H. Rust, and T. M. Butler. Synoptic and meteorological
417 drivers of extreme ozone concentrations over Europe. *Submitted for Publication*, 2015.

418 N. Passant. Speciation of UK emissions of non-methane volatile organic compounds. Technical
419 report, DEFRA, Oxon, UK., 2002.

420 George Pouliot, Hugo A.C. Denier van der Gon, Jeroen Kuenen, Junhua Zhang, Michael D. Moran,
421 and Paul A. Makar. Analysis of the emission inventories and model-ready emission datasets of
422 Europe and North America for phase 2 of the AQMEII project. *Atmospheric Environment*, 115:
423 345–360, 2015.

424 S. E. Pusede, D. R. Gentner, P. J. Wooldridge, E. C. Browne, A. W. Rollins, K.-E. Min, A. R.
425 Russell, J. Thomas, L. Zhang, W. H. Brune, S. B. Henry, J. P. DiGangi, F. N. Keutsch, S. A.
426 Harrold, J. A. Thornton, M. R. Beaver, J. M. St. Clair, P. O. Wennberg, J. Sanders, X. Ren,
427 T. C. VandenBoer, M. Z. Markovic, A. Guha, R. Weber, A. H. Goldstein, and R. C. Cohen.
428 On the temperature dependence of organic reactivity, nitrogen oxides, ozone production, and

the impact of emission controls in San Joaquin Valley, California. *Atmospheric Chemistry and Physics*, 14(7):3373–3395, 2014.

Sally E. Pusede, Allison L. Steiner, and Ronald C. Cohen. Temperature and Recent Trends in the Chemistry of Continental Surface Ozone. *Chemical Reviews*, 115(10):3898–3918, 2015.

D. J. Rasmussen, Jianlin Hu, Abdullah Mahmud, and Michael J. Kleeman. The ozone–climate penalty: Past, present, and future. *Environmental Science & Technology*, 47(24):14258–14266, 2013. PMID: 24187951.

Andrew Rickard, Jenny Young, M. J. Pilling, M. E. Jenkin, Stephen Pascoe, and S. M. Saunders. The Master Chemical Mechanism Version MCM v3.2. <http://mcm.leeds.ac.uk/MCMv3.2/>, 2015. [Online; accessed 25-March-2015].

Juli I. Rubin, Andrew J. Kean, Robert A. Harley, Dylan B. Millet, and Allen H. Goldstein. Temperature dependence of volatile organic compound evaporative emissions from motor vehicles. *Journal of Geophysical Research: Atmospheres*, 111(D3), 2006. D03305.

S. M. Saunders, M. E. Jenkin, R. G. Derwent, and M. J. Pilling. Protocol for the development of the Master Chemical Mechanism, MCM v3 (Part A): tropospheric degradation of non-aromatic volatile organic compounds. *Atmospheric Chemistry and Physics*, 3(1):161–180, 2003.

J. L. Schnell, M. J. Prather, B. Josse, V. Naik, L. W. Horowitz, P. Cameron-Smith, D. Bergmann, G. Zeng, D. A. Plummer, K. Sudo, T. Nagashima, D. T. Shindell, G. Faluvegi, and S. A. Strode. Use of north american and european air quality networks to evaluate global chemistry–climate modeling of surface ozone. *Atmospheric Chemistry and Physics*, 15(18):10581–10596, 2015.

Sanford Sillman. The use of NO_y, H₂O₂, and HNO₃ as indicators for ozone-NO_x-hydrocarbon sensitivity in urban locations. *Journal of Geophysical Research: Atmospheres*, 100(D7): 14175–14188, 1995.

Sanford Sillman. The relation between ozone, NO_x and hydrocarbons in urban and polluted rural environments. *Atmospheric Environment*, 33(12):1821 – 1845, 1999.

Sanford Sillman and Perry J. Samson. Impact of temperature on oxidant photochemistry in urban, polluted rural and remote environments. *Journal of Geophysical Research: Atmospheres*, 100(D6):11497–11508, 1995.

457 D. Simpson, A. Benedictow, H. Berge, R. Bergström, L. D. Emberson, H. Fagerli, C. R. Flechard,
 458 G. D. Hayman, M. Gauss, J. E. Jonson, M. E. Jenkin, A. Nyíri, C. Richter, V. S. Semeena,
 459 S. Tsyro, J.-P. Tuovinen, Á. Valdebenito, and P. Wind. The EMEP MSC-W chemical transport
 460 model – technical description. *Atmospheric Chemistry and Physics*, 12(16):7825–7865, 2012.

461 William R. Stockwell, Paulette Middleton, Julius S. Chang, and Xiaoyan Tang. The second
 462 generation regional acid deposition model chemical mechanism for regional air quality modeling.
 463 *Journal of Geophysical Research: Atmospheres*, 95(D10):16343–16367, 1990.

464 William R. Stockwell, Frank Kirchner, Michael Kuhn, and Stephan Seefeld. A new mechanism
 465 for regional atmospheric chemistry modeling. *Journal of Geophysical Research: Atmospheres*,
 466 102(D22):25847–25879, 1997.

467 E. von Schneidemesser, J. Coates, A. J. H. Visschedijk, H. A. C. Denier van der Gon, and T. M.
 468 Butler. Variation of the NMVOC speciation in the solvent sector and the sensitivity of modelled
 469 tropospheric ozone. *Submitted for Publication*, 2015.

470 Patrick Wagner and Wilhelm Kuttler. Biogenic and anthropogenic isoprene in the near-surface
 471 urban atmosphere — A case study in Essen, Germany. *Science of The Total Environment*, 475:
 472 104 – 115, 2014.

473 Greg Yarwood, Sunja Rao, Mark Yocke, and Gary Z. Whitten. Updates to the Carbon Bond
 474 Chemical Mechanism: CB05. Technical report, U. S Environmental Protection Agency, 2005.